Effects of Control Structure on Performance for an Automotive Powertrain With a Continuously Variable Transmission

Sharon Liu and Anna G. Stefanopoulou

***Abstract*—The wheel speed control problem of an automotive powertrain equipped with a conventional spark-ignition engine directly connected to a continuously variable transmission (CVT) and an electronic throttle is considered. We revisit the seminal work by Guzzella and Schmid and show that the control structure that dedicates the throttle actuator to maintaining engine operation at the maximum fuel efficient operating points results in a single-input–two-output (SITO) system that presents a fundamental limitation in the achievable wheel speed response. The limitation arises from the nonminimum phase (NMP) zero in the transfer function from the CVT ratio rate to the vehicle wheel speed. We relax the requirements on the fuel efficient operation and employ the electronic throttle as a second actuator for the wheel speed regulation problem. The resulting two-input–two-output (TITO) control structure is then analyzed to determine how to mitigate the limitations associated with the NMP zero. Simulations show that the multivariable strategy improves the system performance because it produces minimum phase (MP) behavior without large transient deviations from the optimal fuel economy operation.**

***Index Terms*—Automotive control, continuously variable transmission (CVT) powertrain, controller structure, performance limitations.**

NOMENCLATURE

r	Powertrain speed ratio.
ω_e	Engine speed.
ω_w	Wheel speed.
T_{eb}	Brake engine torque.
T_w	Wheel torque.
T_{ind}	Indicated torque.
c_{ef}	Coefficient of engine friction.
I_e	Engine inertia.
I_w	Effective car inertia at the wheels.
$c_{1,2,3,4}$	Constant polynomial coefficients.
m_a	Cylinder air charge mass.
τ_{bd}	Engine breathing dynamics time constant.
ϑ	Throttle command.
β	Driving surface incline.
C_F	Tire friction coefficient.
C_D	Air drag coefficient.
T_l	Effective vehicle torque load.
W_c	Vehicle weight.
OOL	Optimum operating line.
$\Gamma(\omega_e(t))$	Specific OOL.
x^o	Desired steady-state value.
α_p	Driver pedal position.
$\tilde{\alpha}_p$	Scaled driver pedal position.
$\mathbf{S}_I$	Sensitivity transfer function.
$\mathbf{T}$	Complementary sensitivity transfer function.
rd	Relative degree.

Manuscript received May 22, 2001. Manuscript received in final form December 20, 2001. Recommended by Associate Editor F. Svaricek. This work was supported by the National Science Foundation under Contract ECS-0049025. The work of S. Liu was supported by General Motors.

S. Liu is with Advanced Propulsion System Controls, General Motors Powertrain, Milford, MI 48380-3726 USA (e-mail: sharon.liu@gm.com).

A. G. Stefanopoulou is with the Department of Mechanical Engineering, University of Michigan, Ann Arbor, MI 48109-2125 USA.

Publisher Item Identifier 10.1109/TCST.2002.801881.

I. INTRODUCTION

MANY continuously variable transmission (CVT) designs are being realized in the automotive industry today: [1], [2] use variable stroke drives; [3] designs a nutating tractive drive; [4] develops a toroidal tractive drive directly connected to a spark ignited (SI) engine; [5] interfaces a variable speed pulley drive with an electromagnetic clutch; [6] connects their pulley drive directly to the SI engine; [6]–[8] have pulley drives designed with conventional hydraulic torque converters; [9] puts a pulley drive behind a diesel engine, and [10] and [11] use a pulley drive in a hybrid electric vehicle. A historical perspective of CVT mechanical development is found in [12].

While the mechanical development of CVT devices has matured, CVT powertrain control design is still actively being researched. Together with the use of electronic throttle actuators, the primary benefit of CVT devices (its continuously varying ratio) lets the engine operate independently of any load. In principle, this flexibility allows the fuel economy to be optimized without degrading the acceleration performance [13], but optimizing every operating condition, from launch to engine braking, is not trivial [6], [14], [15]. The experienced observations of [16] suggest potential for improvements in the CVT controls.

When electronic throttle actuators are used, a strategy is needed to convert the driver pedal position input into an operating command [6], [14], and [15]. The strategy can be a static feedforward map from pedal position to the desired vehicle performance. A fuel economy objective can then be used to determine the desired engine operation corresponding to the desired vehicle performance through an appropriate choice of the CVT ratio. The literature covers many different strategies [6]–[10], [14], [15], [17].

The desired CVT powertrain transient specifications are usually determined for different performance objectives and always include either a warning to monitor [4], [6], [14] or limits on the CVT ratio rate [15], [7]. This is because the wheel speed equation of motion shows that the ratio rate input opposes the throttle input. This characteristic is equivalent to a nonminimum phase (NMP) zero in the transfer function from the ratio rate input to the wheel speed output when the

system model is linearly approximated [10]. NMP behavior is undesirable because, first, the initial transient step response of a stable linear system with one real NMP zero starts in the wrong direction and has initial undershoot. Second, feedback cannot remove NMP zeros. Third, open-loop systems with NMP zeros have closed-loop performance limitations that are well documented, i.e., [18], [19], and their references. Hence, to achieve all desired control objectives, the engine and CVT subsystems must be dynamically coordinated [8].

Some commercial applications avert any NMP behavior by employing additional power sources to compensate the initial inverse response. For example, [26] and [27] use energy stored in a flywheel to passively compensate for the initial inverse wheel speed response. Using nonlinear inverse dynamics, [25] cancels the ratio change effect on the wheel speed with the electric motor in the Eidgenössische Technische Hochschule (ETH) hybrid electric powertrain. In a different discussion about this hybrid electric vehicle, fuel efficiency is maximized by dedicating the throttle actuator to controlling the engine on a fuel optimum speed-load trajectory. The ratio rate is then used solely to govern the vehicle acceleration. To avoid bandwidth limitations associated with the NMP response of the output feedback single-input–single-output (SISO), [10] uses a nonlinear state feedback single-input–two-output (SITO) architecture.

The first result we present here clarifies that the initial inverse response cannot be eliminated by using additional measurements and the undesirable behavior persists unless the ratio rate is detuned considerably. It is thus shown that the controller architecture that dedicates the throttle actuator to ensure the fuel economy objectives and the CVT to meet the driveability objectives presents a stringent tradeoff between the fast wheel speed response and initial monotonic wheel speed response. To mitigate this tradeoff, we relax the transient fuel economy requirements and investigate if a two-input–two-output (TITO) controller that coordinates both throttle and ratio rate commands can achieve better driveability performance. Since it is well known that the multivariable multiple-input–multiple-output (MIMO) controller structure plays an important role in achieving a better tradeoff between various performance objectives when fundamental limitations are present [20], [23], we investigate a decentralized and a fully centralized (multivariable) controller structure.

Our second result is that a low-order decentralized TITO controller *cannot* alleviate the above tradeoff between fast and monotonic wheel speed response associated with the NMP zero, unless the throttle can affect engine torque instantaneously. This is unrealistic with conventionally throttled gasoline engines, hence, we postulate that a fully multivariable (centralized) TITO structure is a better solution.

Our final result shows that, indeed, the multivariable controller structure provides the degrees of freedom to achieve fast and monotonic wheel speed response. In addition, we identify the exact mechanism with which a cross coupling term of the multivariable controller achieves the performance objectives.

Our results are independent of control design methodology and specific plant (engine/CVT) parameters. Thus, they can be used early in the system design process. The design implications of our controller structure analysis can be summarized as follows. One should not relax the transient fuel economy requirements if a coordinated (multivariable) TITO controller structure cannot be used in the final vehicle implementation. It is also evident that one should explore the inexpensive software solution of the multivariable controller structure before increasing the mechanical system complexity by employing a supplemental torque source configuration (electric motor, flywheel, etc.) in order to alleviate the initial inverse wheel speed response.

This paper is organized as follows: The assumptions used to model the system of interest, the control objectives, and the derivation of the system open-loop state space are presented in Section II. Since the electronic throttle actuator is coordinated with ratio rate as an input, the engine breathing dynamics are also modeled. The relationship between the desired optimum fuel consumption trajectory, the driver input interpretation, and the state tracking reference is explained in Section III. The linearization of the model about the reference steady states result in a TITO realization described in Section IV. Constraining the engine to operate on the optimum fuel consumption trajectory at all times reduces the TITO system to an SITO problem. The resulting limitations for this approach are discussed in Section V. To overcome some of these limitations, the TITO system is constrained to operate on the optimum fuel consumption trajectory only at steady state. Low-order decentralized and multivariable controllers are applied to the TITO system, in Section VI, and their ability to achieve the control objectives are compared. Examples of closed-loop responses to "kick-down" commands are included in this section. They illustrate the role of the closed-loop architecture in the inevitable tradeoff between wheel acceleration performance and fuel economy. Conclusions and suggestions for future investigations are discussed in Section VII.

II. Model

Standing assumptions for the system are

- spark-ignition internal combustion engine generates power;
- CVT directly connects the engine to the wheels;
- CVT device is modeled as an integrator based on the assumption that an internal controller generates its response;
- no slip across the powertrain.

The first three assumptions coincide with the conditions imposed in [10]. The last assumption ensures that (1) holds. Let the powertrain speed ratio be defined as

$$r = \frac{\omega_e}{\omega_w} = \left(\frac{T_{eb}}{T_w}\right)^{-1} \tag{1}$$

where ω_e is the engine speed, ω_w is the vehicle wheel speed, T_{eb} is the brake engine torque, and T_w is the wheel torque. Notice that when the engine brake torque is zero, and the vehicle speed is zero, for example when the engine idles with zero vehicle speed, the speed ratio is infinite in (1). Operations near this condition will not be addressed.

The powertrain model is based on the relationship described by (1). The brake engine torque T_{eb} is the indicated engine torque T_{ind} minus frictional losses and the inertial torque. The indicated engine torque can be approximated as a function that

is linear in the mass of air charge into the cylinders m_a, and is quadratic in the engine speed ω_e

$$T_{eb} = T_{ind} - c_{ef}\omega_e^2 - I_e\dot{\omega}_e$$
$$T_{ind} = c_1 + c_2 m_a + c_3\omega_e + c_4\omega_e^2. \quad (2)$$

For the analysis, the manifold filling dynamics, throttle actuator dynamics, and induction to power delay are lumped into a single linear first-order lag with time constant $\tau_{bd} = 0.07$ s, from the throttle command ϑ, to the cylinder air charge m_a

$$\dot{m}_a = \frac{1}{\tau_{bd}}(\vartheta - m_a). \quad (3)$$

Note that if we assume the worst case pure time delay for the slowest engine speed of interest to be 0.03 s then a lag of 0.027 s in series produces the same phase lag as the 0.07-s time lag we use in our analysis and simulations. Additionally, the rational Pade approximation of a time delay does not change the relative degree arguments that we employ in the following analysis in Sections VI and VII.

The tractive torque in (1) T_w drives the wheels and includes the vehicle load. The vehicle load consists primarily of air drag, vehicle weight on the driving surface incline β, and tire friction resistance [22]. The tire friction coefficient C_F, air drag coefficient C_D, and the vehicle weight W_c have known nominal values. Only the forward driving operations are considered

$$T_w = I_w\dot{\omega}_w + T_l$$
$$T_l = C_F W_c\cos\beta + W_c\sin\beta + C_D\omega_w^2. \quad (4)$$

Using the time derivative of (1), $\dot{\omega}_e = \dot{r}\omega_w + r\dot{\omega}_w$, then substituting expressions from (2)–(4) into (1), the wheel acceleration can be solved in terms of wheel speed (see the Appendix). The system state space is described in (5) when the ratio, the wheel speed, and the cylinder air charge are chosen as states $x = [r\ \omega_w\ m_a]^T$, and the ratio rate and the throttle command are chosen as inputs $u = [\dot{r}\ \vartheta]^T$

$$\dot{x} = \begin{bmatrix} f_1 \\ f_2 \\ f_3 \end{bmatrix} + \begin{bmatrix} 1 & 0 \\ g_1 & 0 \\ 0 & \dfrac{1}{\tau_{bd}} \end{bmatrix} u, \qquad y = \begin{bmatrix} r \\ \omega_w \end{bmatrix}$$
$$f_1 = 0$$
$$f_2 = \frac{[(c_4 - c_{ef})x_1^3 - C_D]x_2^2 + c_3 x_1^2 x_2 + [(c_1 + c_2 x_3)x_1 - \overline{\beta}]}{I_w + I_e x_1^2}$$
$$f_3 = -\frac{1}{\tau_{bd}}x_3$$
$$g_1 = -\frac{I_e x_1 x_2}{I_w + I_e x_1^2}, \qquad \overline{\beta} = C_F W_c\cos\beta + W_C\sin\beta. \quad (5)$$

The state equation for wheel acceleration $\dot{x}_2$ shows that the ratio rate input u_1 opposes the throttle input or mass air charge response $x_3 = m_a$, because $(c_1 + c_2 x_3)x_1$ is positive for all x_1 and x_3, and g_1 is negative for all $I_e x_1 x_2$ in the forward driving range. The control problem is to track the desired wheel speed and ratio. The desired steady-state conditions are discussed in the next section.

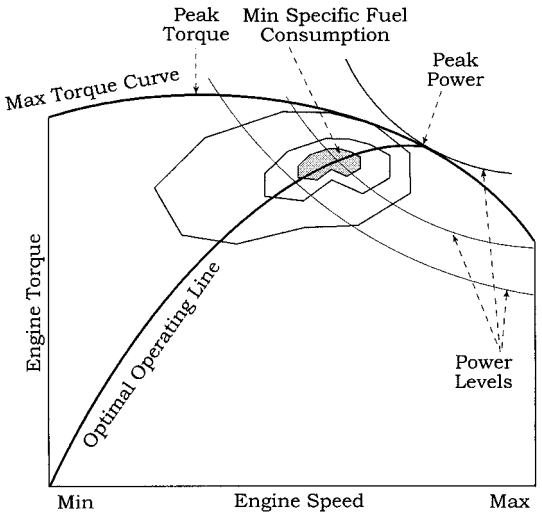

Fig. 1. OOL on a generic engine characteristics map.

III. Optimum Operations

We consider a small "kick-down" maneuver as the evaluation criteria, similar to [10]. This maneuver is a driver imposed acceleration demand that requires both an engine torque increase and a transmission ratio change. The closed-loop control objective is to achieve stable, monotonic wheel speed response with zero steady-state tracking error to a "kick-down" command.

Moreover, we consider a line that represents the minimum brake specific fuel consumption for every brake engine power level on the generic engine characteristics map shown in Fig. 1. This line is coined the OOL in [21] because, in general, it can be chosen to represent the ideal engine operations prescribed by the powertrain designer. For convenience, the term OOL is adopted here. For consistency with [10], the OOL is defined as $\Gamma(\omega_e(t))$; to achieve maximum fuel efficient operations, the desired steady-state engine operating points are along $\Gamma(\omega_e(t))$.

The OOL can be described by a one-to-one map of the desired steady-state engine speed ω_e^o and the desired steady-state engine torque $T_e^o = \Gamma(\omega_e(t))$. This trajectory is always maintained by some control strategies, such as [10]. It is used only as the desired steady-state reference trajectory in the current study. For example, if the driver pedal position input α_p were interpreted as a desired power level [6], then the desired steady-state engine speed ω_e^o and the desired steady-state mass air flow m_a^o can be found by using the definition of power, $\Gamma(\omega_e(t))$, (2), and (3). With no slip across the powertrain, the desired engine power is equal to the desired output power at the wheels. Therefore, using the definition of power with (1) and (4), the desired steady-state wheel speed ω_w^o and the desired steady-state ratio r^o are determined. In the following linearization and analysis, $C_o = [\alpha_r\ \ 1]^T$ is the smooth transformation which maps the scaled driver pedal position input or command $\tilde{\alpha}_p$ to the reference state $[r^o\ \omega_w^o\ m_a^o]^T = x^o$.

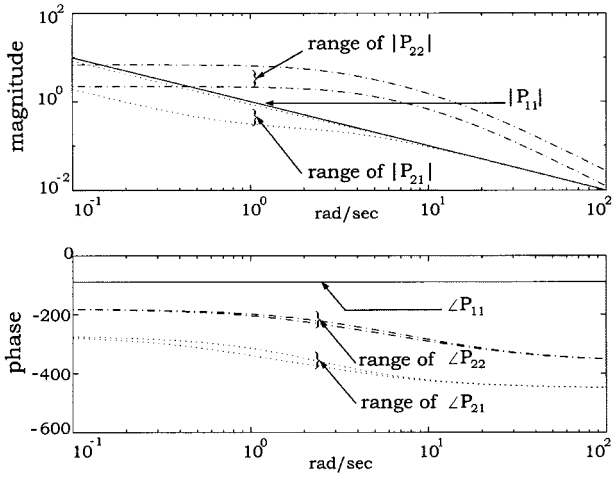

Fig. 2. Bode plots of the transfer function elements in (6).

IV. Linearization

The transfer function of (5) linearized about the steady state x^o is

$$P(s) = \begin{bmatrix} \dfrac{1}{s} & 0 \\ \dfrac{\left(g_1(x^o)s + \dfrac{\partial f_2}{\partial x_1}\Big|_{x^o}\right)}{s\left(s - \dfrac{\partial f_2}{\partial x_2}\Big|_{x^o}\right)} & \dfrac{\dfrac{\partial f_2}{\partial x_3}\Big|_{x^o}\dfrac{1}{\tau_{bd}}}{\left(s - \dfrac{\partial f_2}{\partial x_2}\Big|_{x^o}\right)\left(s + \dfrac{1}{\tau_{bd}}\right)} \end{bmatrix}. \tag{6}$$

The controller inputs are the ratio rate and the throttle command. The measured outputs are the ratio and wheel speed. For all x^o, $g_1(x^o) < 0$; $\partial f_2/\partial x_1|_{x^o} > 0$; $\partial f_2/\partial x_2|_{x^o} < 0$; $\partial f_2/\partial x_3|_{x^o} > 0$; $\tau_{bd} > 0$.

There is a NMP zero in P_{21} which maps $\dot{r} \to \omega_w$. This is apparent in the Bode plots of the individual transfer functions from (6) shown in Fig. 2 for $\alpha_p = 0.1$ and 0.99. The phase for $\angle P_{21}$ is not minimum, with an additional 90° lag. However, the coprime factorization of (6) contains no multivariable transmission zeros. The frequency gain plot in Fig. 2 shows that there is considerable interaction between the impulse response of each output to each input and that the bandwidth of P_{22} is important for rejecting the disturbances from the CVT dynamics. These open-loop characteristics for (6) represent a TITO structure, from the ratio rate and throttle inputs to the ratio and wheel speed outputs. In the next section, we show how the authors in [10] formulate a SITO control problem by dedicating the throttle actuator to ensure engine operation at the OOL. We also analyze the pertinence of the SITO architecture limitations.

V. SITO Architecture

The optimum fuel objectives are achieved if the engine torque satisfies $T_e(t) = T_e^d = \Gamma(\omega_e(t))$. The electronic throttle ϑ can be controlled to ensure that the engine torque tracks this desired Γ curve for all engine speeds. Similar to [10, Fig. 2], Fig. 3 illustrates the architecture for this approach. The authors there use an instantaneous mass of air charge response m_a to the command ϑ that satisfies $T_e(t) = \Gamma(\omega_e(t))$ based on (2) and (3). The throttle control C_2 reacts only to changes in the engine speed caused by the drivetrain, through CVT command or load disturbances. Due to the inertial rotational dynamics, these changes in engine speed are much slower than the engine breathing or combustion dynamics $\vartheta \to T_e$. Hence, by the principle of frequency separation, a fast closed-loop system in m_a can easily track the slowly varying $\Gamma(\omega_e(t))$ trajectory and maintain engine operation on the OOL, i.e., maintain $T_e(t) = \Gamma(\omega_e(t))$. The control problem is then posed by a SISO wheel speed tracking problem controlled by the CVT ratio rate.

Guzzella and Schmid avoids the closed-loop bandwidth limitations associated with the NMP zero by utilizing an additional measurement, namely, the CVT ratio, to form the SITO system shown in Fig. 4. This SITO system does not have NMP MIMO transmission zeros; thus there is no bandwidth limitation associated with the SITO plant. However, one can show that any stable closed-loop transfer function from $\tilde{\alpha}_p$ to ω_w that uses $\dot{r}$ for the single actuator will still have the NMP zero. Thus, the wheel speed will exhibit the undesirable inverse response even when extra sensors are employed. Recall that internal stability of the feedback system prohibits cancellation of the NMP zero. The complementary sensitivity function of the system in Fig. 4 shows that the NMP zero must affect the wheel speed independently of the control algorithm for $\dot{r}$.[1]

$$\begin{aligned} \frac{\omega_w}{\tilde{\alpha}_p} &= P_{21}(1 + C_{12}P_{21} + C_{11}P_{11})^{-1}(\alpha_r C_{11} + C_{12}) \\ &= P_{21}\mathbf{S}_I(\alpha_r C_{11} + C_{12}) \\ &= \mathbf{T} \end{aligned} \tag{7}$$

where $z > 0$ is the real NMP zero, $\mathbf{T}(z) = 0$, and $\mathbf{S}_I(z) = 1 - \mathbf{T}(z) = 1$. Due to the interpolation constraints, the wheel speed step response will satisfy the following relationship:

$$\int_0^\infty e^{-zt}\omega_w(t)\,dt = 0. \tag{8}$$

Since $e^{-zt} > 0$, it follows that $\omega_w(t) < 0$ for some time interval so that the wheel speed will exhibit undershoot. The above holds for all control signals that are bounded integrable functions. Per [24], the undershoot is unavoidable even if the controller is nonlinear or time varying.

Moreover, the Poisson integral constraints hold and impose sensitivity peaking to counterbalance the aggressive sensitivity decrease at some frequencies. This sensitivity peaking needs to be carefully assessed both in terms of stability and transient performance.

While adding measurements for the inner loops may not remove the NMP behavior, changing the powertrain control strategy does. By relaxing the requirement of engine operation at the OOL curve ($T_{eb} = \Gamma(\omega_e)$), the throttle ϑ can be used as an additional actuator for tracking the desired wheel speed. Fuel efficiency is thus traded for driveability. The throttle now must be coordinated with the CVT ratio rate, and the breathing dynamics become important because the engine torque is used to compensate fast transient wheel acceleration.

[1]Dependence on the complex variable s has been omitted for legibility.

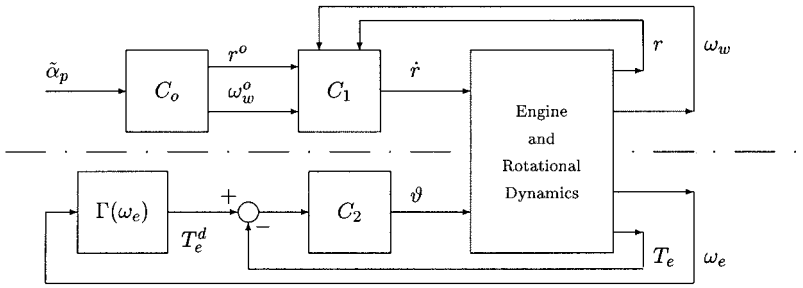

Fig. 3. CVT powertrain control system block diagram.

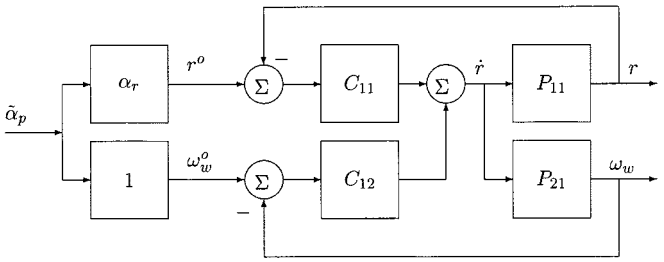

Fig. 4. SITO form of Fig. 3.

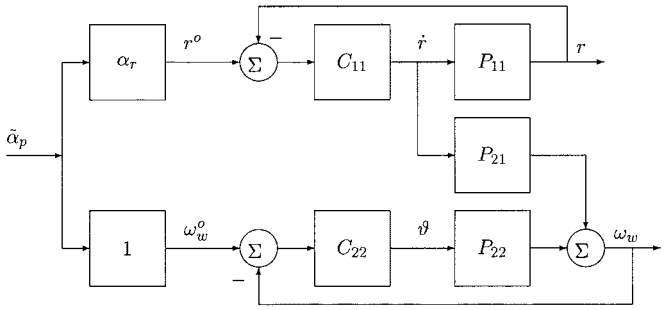

Fig. 5. Decentralized controller with the TITO system.

The third-order TITO system of interest is given by (5). The effects of the choice of the multivariable controller architecture on the TITO system performance are investigated in the next section.

VI. Effects of TITO Controller Structure

In the previous section, we showed that the coordination of throttle and ratio rate might be critical in alleviating the inverse response of the wheel speed. Significant coupling of the resulting system at the frequencies of interest is shown by the Bode plots in Fig. 2. This suggests that a fully centralized multivariable controller has the capability to coordinate both throttle and ratio rate.

To verify this hypothesis, we specifically investigate a multivariable controller based on the wheel speed and ratio error in a unity feedback configuration. This configuration is practically the automotive industry standard. Another automotive industry standard is the use of decentralized (diagonal) control algorithms of the lowest possible order. These practices are necessary due to stringent implementation and calibration constraints. Hence, the effectiveness or potential fundamental limitations of decentralized controllers as well as the role of controller order are also considered for the current problem.

A. Decentralized Structure

We consider the proposed decentralized controller $C = \mathrm{diag}(C_{11}, C_{22})$ that is depicted in Fig. 5. The wheel speed is given by

$$\omega_w(s) = \frac{\alpha_r P_{21}C_{11} + P_{22}C_{22} + P_{11}C_{11}P_{22}C_{22}}{(1 + P_{11}C_{11})(1 + P_{22}C_{22})}\,\tilde{\alpha}_p. \quad (9)$$

Let C_{11} and C_{22} be causal and realizable controllers that achieve closed loop stability. For minimum phase (MP) behavior we require that the initial value of the derivative of the wheel speed be positive during a step change in pedal position command

$$\dot{\omega}_w(t=0) = \lim_{s\to\infty} s^2\omega_w(s) > 0. \quad (10)$$

In the limit as $s \to \infty$, the denominator of $\omega_w(s)$ in (9) is one. After applying a unit step input, the limit as $s \to \infty$ for the numerator of $s^2\omega_w(s)$ is

$$\lim_{s\to\infty} s(\alpha_r P_{21}C_{11} + P_{22}C_{22} + P_{11}C_{11}P_{22}C_{22}). \quad (11)$$

For stability and steady-state tracking reasons, C_{11} must have positive coefficients. It is thus not possible to change the sign of the component of the initial response that contributes to the inverse behavior ($\alpha_r P_{21}C_{11}$) by manipulating the sign of the controller C_{11}. Consequently, the initial wheel speed response is dominated by the path with the smallest pole-zero excess, relative degree (rd), or the fewest number of integrations.

From (6) and Fig. 2, the relative degree of each portion of the system transfer function can be determined as $rd(P_{11}) = 1$, $rd(P_{21}) = 1$, and $rd(P_{22}) = 2$. Due to its high relative degree, the component $P_{11}C_{11}P_{22}C_{22}$ does not contribute to the initial response. To compensate the inverse response due to the NMP zero in P_{21}, it is important to design a decentralized controller so that the relative degree of the upper path (through the NMP contributions) is larger than the relative degree of the lower path

$$\begin{aligned} rd(P_{21}C_{11}) \geq rd(P_{22}C_{22}) \Rightarrow \\ rd(P_{21}) + rd(C_{11}) \geq rd(P_{22}) + rd(C_{22}) \Rightarrow \\ rd(C_{11}) \geq rd(C_{22}) + 1. \end{aligned} \quad (12)$$

As one can see, a proportional (P), proportional-integral (PI) diagonal controller does not satisfy condition (12). We are interested in the P, PI controller because it provides the lowest

order decentralized controller that permits output tracking with zero steady-state error. Indeed, because the ratio output is the integral of the ratio rate input, a proportional feedback gain for this loop suffices to track the desired reference ratio r^o. For the wheel speed to track the desired reference ω_w^o, C_{22} must include an integrator.

Note that condition (12) is satisfied if C_{11} is a lag. Introducing a lag in the C_{11} term will eliminate the inverse response of the ω_w but can potentially slow down the closed-loop response in the upper loop. A similar effect can be achieved if we prefilter the command α_r before the feedback loop. This result sheds light on an important limitation of the decentralized controller architecture. Namely, a decentralized controller imposes a tradeoff between fast ratio rate and initial monotonic wheel speed response.

Another important observation is that if the breathing dynamics is negligible in the P_{22} term, then the relative degree condition for the MP response is modified

$$rd(C_{11}) \geq rd(C_{22}). \tag{13}$$

The new condition is satisfied by a P, PI decentralized controller without the need to slow down the upper loop. As one expects, fast dynamics from $\theta \rightarrow \omega_w$ can potentially compensate for the initial inverse response from $\dot{r} \rightarrow \omega_w$. This has also been verified numerically.

B. Multivariable

It is of interest to investigate if a fully centralized multivariable controller can mitigate the tradeoff between fast ratio rate and monotonic initial wheel speed associated with the decentralized controller architecture that we analyzed in the previous section. When a fully centralized multivariable controller is considered for the TITO system, the wheel speed is given by (14), shown at the bottom of the page.

The lowest order multivariable controller that achieves the steady-state tracking requirement uses P, P, P, PI for the C_{11}, C_{12}, C_{21}, C_{22} controllers, respectively. For MP behavior, we require that the initial value of the derivative of the wheel speed be positive during a step change in pedal position command, as in (10). In the limit, as $s \rightarrow \infty$, the denominator of $\omega_w(s)$ is again one. After applying the step input, the numerator of $s^2\omega_w(s)$ is

$$\lim_{s\rightarrow\infty} s[P_{21}(\alpha_r C_{11} + C_{12}) + P_{22}(\alpha_r C_{21} + C_{22}) + P_{11}P_{22}(C_{11}C_{22} - C_{12}C_{21})]. \tag{15}$$

Using the plant in (6), the initial wheel acceleration is defined by

$$\dot{\omega}_w(t=0) = g_1(x^o)(\alpha_r C_{11} + C_{12}). \tag{16}$$

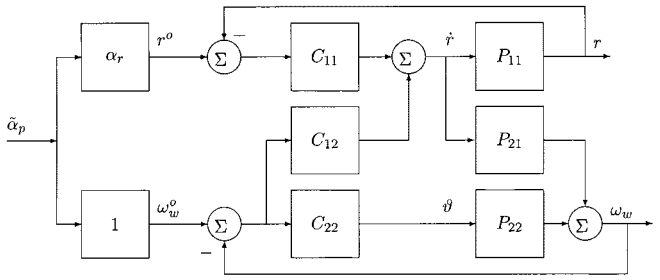

Fig. 6. Reduced multivariable controller (where $C_{21} = 0$) with the TITO system.

By choosing C_{11} and C_{12} such that

$$\alpha_r C_{11} + C_{12} \leq 0 \tag{17}$$

the initial inverse response caused by the NMP zero in P_{21} can be eliminated independently of the order of the multivariable controller or the methodology for its design. Thus, the following summarizes the important points.

1) The multivariable controller does not present any limitation in achieving fast ratio rate response and a monotonic initial wheel speed.
2) The C_{12} term is the important cross coupling term that enables the multivariable controller to mitigate the limitations of the decentralized architecture. It provides the mechanism with which the ratio rate command utilizes the errors of both outputs to avoid degradation in the lower loop.

The structure of the controller interaction with the plant is shown in Fig. 6.

To illustrate these findings, one set of fixed gains for the P, P, P, PI multivariable controller is found to compensate the linearized system for various steps of driver pedal positions. In particular, the constants are chosen such that $\alpha_r C_{11} + C_{12} = 0$. The time responses are plotted in Fig. 7 as the heavy solid lines, showing no initial inverse for either the wheel speed or ratio and very good performance. The different step sizes are 10–20%, 60–75%, 30–90%, and 10–99%. The 60–75% step response is comparable to the example command used in [10]. Notably, increasing the step size causes the response to overshoot. With some tuning, the gains can be scheduled for various step sizes over different operating conditions to optimize each time response. The lighter lines in these plots represent the nonlinear system compensated by the same linear controller with the same fixed gains in response to the same four different driver pedal positions. For smaller step commands, such as the 10–20% and 60–75%, the linearized and nonlinear system output responses are indistinguishable. When the step command is large, the nonlinear system response is significantly slower than the linearized system response.

The phase trajectories from the nonlinear simulations are plotted in Fig. 8 on the engine characteristics map. By relaxing

$$\omega_w = \frac{P_{21}(\alpha_r C_{11} + C_{12}) + P_{22}(\alpha_r C_{21} + C_{22}) + P_{11}P_{22}(C_{11}C_{22} - C_{12}C_{21})}{1 + P_{11}C_{11} + P_{21}C_{12} + P_{22}C_{22} + P_{11}P_{22}(C_{11}C_{22} - C_{12}C_{21})}\,\tilde{\alpha}_p. \tag{14}$$

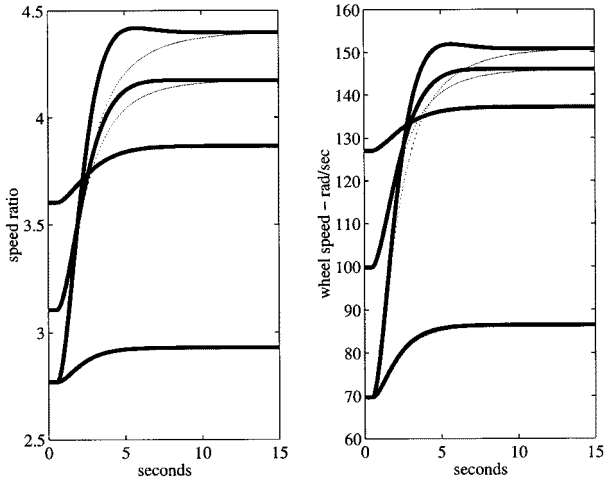

Fig. 7. Ratio and wheel speed time responses to different "kick-down" maneuvers.

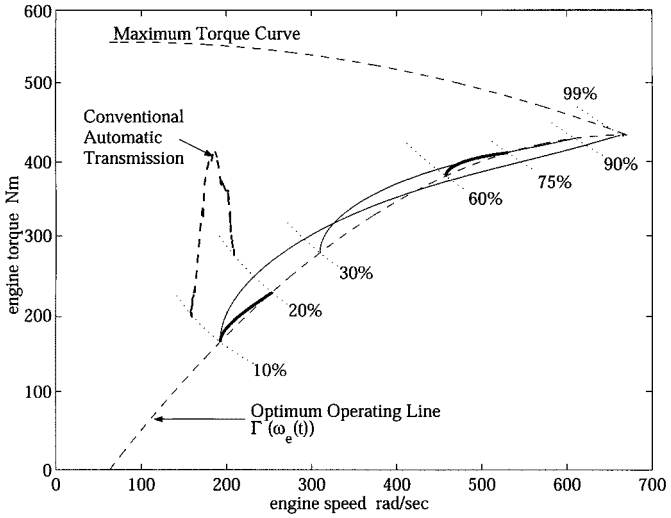

Fig. 8. Phase portrait of simulated responses on the engine characteristics map.

the requirement to maintain optimum engine operations, the unconstrained mass air flow causes the engine transient to deviate from the $\Gamma(\omega_e(t))$ curve. Remarkably, despite the use of the lowest order linear tracking multivariable controller with fixed gains for all operating conditions, the deviation is not very large even for large step commands. The heavy dashed and jagged line is a comparison of a 10–20% pedal position response of a conventional automatic transmission which does not satisfy the $\Gamma(\omega_e(t))$ curve even at steady state.

VII. Conclusion

This paper shows that the SITO approach, which guarantees the engine to operate on the prescribed $\Gamma(\omega_e(t))$ curve, always results in initial wheel speed undershoot in response to a step driver pedal position command. By relaxing the transient engine operating requirement to stay on the $\Gamma(\omega_e(t))$ curve, the throttle can be used to compensate this wheel speed initial undershoot, but the lowest order decentralized tracking controller with the TITO approach cannot achieve both a stable and montonic wheel speed response. A decentralized controller that achieves the desired wheel speed performance must slow down the ratio controller. Alternatively, an appropriate choice for the off-diagonal term C_{12} of the multivariable controller can cancel the NMP effect of ratio rate on the wheel speed initial response without slowing down the ratio controller. In fact, the lowest order constant linear multivariable tracking controller is shown for various examples to achieve good wheel acceleration performance without significantly deviating from the transient objective: the $\Gamma(\omega_e(t))$ curve. Experimental verification and robustness analysis of the multivariable TITO controller will be pursued in future work.

Appendix

Assume there is no slip across the entire powertrain. The speed ratio is defined in (1) as

$$r = \frac{\omega_e}{\omega_w} = \left(\frac{T_{eb}}{T_w}\right)^{-1}. \tag{18}$$

Its time derivative is

$$\dot{\omega}_e = \dot{r}\omega_w + r\dot{\omega}_w. \tag{19}$$

Fit the indicated/generated torque as a second-order polynomial function in engine speed

$$T_{ind} = c_1 + c_2 m_a + c_3\omega_e + c_4\omega_e^2. \tag{20}$$

The brake torque, which is the input to the transmission, is the indicated torque minus viscous losses and engine inertia as expressed in (2)

$$\begin{aligned} T_{eb} &= T_{ind} - c_{ef}\omega_e^2 - I_e\dot{\omega}_e \\ &= c_1 + c_2 m_a + c_3\omega_e + (c_4 - c_{ef})\omega_e^2 - I_e\dot{\omega}_e. \end{aligned} \tag{21}$$

The torque driving the wheels is the car inertia plus car load in (4)

$$\begin{aligned} T_w &= I_w\dot{\omega}_w + T_l \\ &= I_w\dot{\omega}_w + C_F W_c\cos\beta + W_c\sin\beta + C_D\omega_w^2. \end{aligned} \tag{22}$$

The car load consists of tire friction, driving surface grade, and air drag $T_l = C_F W_c\cos\beta + W_c\sin\beta + C_D\omega_w^2$. Using the far right-hand side of (1)

$$T_w = rT_{eb} \tag{23}$$

substitute the preceding expressions of torque into the torque ratio and eliminate the engine speed to get

$$\begin{aligned} &I_w\dot{\omega}_w + C_F W_c\cos\beta + W_c\sin\beta + C_D\omega_w^2 \\ &\quad = (c_1 + c_2 m_a)r + c_3 r^2\omega_w + (c_4 - c_{ef})r^3\omega_w^2 - I_e r\dot{\omega}_e. \end{aligned} \tag{24}$$

Substituting (19) for engine acceleration, this expression can be arranged with wheel acceleration terms only on the left-hand side

$$\begin{aligned} &(I_w + I_e r^2)\dot{\omega}_w \\ &\quad = (c_1 + c_2 m_a)r + c_3 r^2\omega_w + (c_4 - c_{ef})r^3\omega_w^2 \\ &\qquad - (C_F W_c\cos\beta + W_c\sin\beta) - C_D\omega_w^2 - I_e r\omega_w\dot{r}. \end{aligned} \tag{25}$$

This yields the standard equation of motion for wheel acceleration of a CVT powertrain

$$\dot{\omega}_w = \frac{[(c_4 - c_{ef})r^3\omega_w^2 - C_D]\omega_w^2 + c_3 r^2 \omega_w + [(c_1 + c_2 m_a)r - \overline{\beta}]}{I_w + I_e r^2} - \frac{I_e r \omega_w}{I_w + I_e r^2}\,\dot{r} \quad (26)$$

that is $\dot{x}_2$ in (5) when the states are $x = [r \;\; \omega_w \;\; m_a]^T$, and $\overline{\beta} = C_F W_c \cos\beta + W_C \sin\beta$. If m_a is predetermined as in the SITO case and $\dot{r}$ is the only input u, then letting

$$\gamma = c_1 + c_2 m_a \qquad a = C_D \qquad \nu = r \qquad \alpha = c_4 - c_{ef}$$
$$\beta' = c_3 \qquad \Theta_e = I_e \qquad c = \overline{\beta} \qquad \eta = 1 \qquad \Theta_w = Iw \quad (27)$$

turns (26) into

$$\dot{\omega}_w = \frac{[\alpha\nu^3 - a]\omega_w^2 + \beta'\nu^2\omega_w + [\gamma\nu - c]}{\Theta_w + \Theta_e\nu^2} - \frac{\Theta\nu\omega_w}{\Theta_w + \Theta_e\nu^2}\,u \quad (28)$$

which is exactly the same as [10, eq. (4)].

REFERENCES

[1] F. A. Fitz, P. B. Pires, and Epilogics, Inc., "A high torque, high efficiency CVT for electric vehicles,", SAE Paper 910 251.

[2] ——, "A geared infinitely variable transmission for automotive applications,", SAE Paper 910 407.

[3] Y. Kemper, L. Elfes, and Vadatec Corp., "A continuously variable traction drive for heavy-duty agricultural and industrial applications,", SAE Paper 810 948.

[4] M. J. Smith, C. J. Greenwood, and G. B. Soar, "A full-toroidal traction drive CVT—From theory to practice," *Int. Mech. Eng.*, 1992.

[5] S. Hirano, A. L. Miller, and K. F. Schneider, "SCVT—A state of the art electronically controlled continuously variable transmission,", SAE Paper 910 410.

[6] H. Vahabzadeh and S. M. Linzell, "Modeling, simulation, and control implementation for a split-torque, geared neutral, infinitely variable transmission,", SAE Paper 910 409.

[7] K. Funatsu, H. Koyama, and T. Aoki, "Electronic control system of Honda for CVT," in *Proc. Int. Conf. Continuously Variable Power Transmissions CVT 1996*, Sept. 11–12, 1996, Conf. Pub. 107.

[8] M. Yasuoka, M. Uchida, S. Katakura, and T. Yoshino, "An integrated control algorithm for an SI engine and a CVT,", SAE Paper 1999-01-0752.

[9] M. Deacon, C. J. Brace, M. Guebeli, N. D. Vaughan, C. R. Burrows, and R. E. Dorey, "A modular approach to the computer simulation of a passenger car powertrain incorporating a diesel engine and continuously variable transmission," in *Proc. Inst. Elect. Eng. Int. Conf. Contr. 1994*, vol. 1, London, U.K., Paper 389.

[10] L. Guzzella and A. M. Schmid, "Feedback linearization of spark-ignition engines with continuously variable transmissions," *IEEE Trans. Contr. Syst. Technol.*, vol. 3, pp. 54–60, Mar. 1995.

[11] A. Schmid, P. Dietrich, S. Ginsburg, and H. P. Geering, "Controlling a CVT-equipped hybrid car,", SAE Paper 950 492.

[12] P. G. Gott, *Changing Gears: The Development of the Automotive Transmission.* Warrendale, PA: SAE, 1991.

[13] K. Newton, W. Steed, and T. K. Garrett, *The Motor Vehicle*, 12th ed. Warrendale, PA: SAE, 1996, pp. 716, 737–743.

[14] C. Chan, D. Yang, T. Volz, D. Breitweiser, F. S. Jamzadeh, A. Frank, and T. Omitsu, "System design and control considerations of automotive continuously variable transmissions,", SAE Paper 840 048.

[15] K. Engelsdorf, K.-H. Senger, and M.-P. Bolz, "Electronic CVT control for power train optimization," in *Proc. Int. Conf. Continuously Variable Power Transmissions CVT 1996*, Sept. 11–12, 1996, Conf. Pub. 111.

[16] N. Liebrand, "Future potential for CVT technology," in *Proc. Int. Conf. Continuously Variable Power Transmissions CVT 1996*, Sept. 11–12, 1996, Conf. Pub. 105.

[17] M. J. Smith, D. H. Ridmarsh, and P. Foss, "The development of high specific output engines for use with a two regime IVT," Autotech 1993, NEC, Birmingham, U.K., C427/36/237.

[18] M. M. Seron, J. H. Braslavsky, and G. C. Goodwin, *Fundamental Limitations in Filtering and Control*. New York: Springer-Verlag, 1997.

[19] J. Freudenberg, R. Middleton, and A. Stefanopoulou, "A survey of inherent design limitations," in *Proc. Amer. Contr. Conf. Workshop Tutorial 2000*, Chicago, IL, June 2000.

[20] A. G. Stefanopoulou, K. R. Butts, J. A. Cook, J. S. Freudenberg, and J. W. Grizzle, "Automotive powertrain control for modular controller architectures: A case study," in *Proc. 1995 Conf. Decision Contr.*, pp. 768–773.

[21] H. Kim, H. Song, T. Kim, and J. Kim, "Metal belt CVT and engine optimal operation by PWM electro-hydraulic control," in *Proc. Int. Conf. Continuously Variable Power Transmissions CVT 1996*, Sept. 11–12, 1996, Conf. Pub. 304.

[22] *Bosch Automotive Handbook*, 3rd ed., 1994, pp. 323–327.

[23] V. Marcopoli, "Inherent limitations associated with the weapon pointing control problem for a tank elevation system," in *Proc. 2000 Amer. Contr. Conf.*, Chicago, IL, June 2000.

[24] R. H. Middleton, "Tradeoffs in linear control system design," *Automatica*, vol. 27, no. 2, pp. 281–292, 1991.

[25] E. Shafai and H. Geering, "Control issues in a fuel-optimal hybrid car," in *Proc. 1996 IFAC 13th Triennial World Congr.*, San Francisco, CA, Session 8b-07 4, pp. 231–236.

[26] A. Serranrens and B. Vroemen, "CVT control: A hierarchical approach," in *Proc. ASME AVEC 2000*, Ann Arbor, MI, no. 134, pp. 619–627.

[27] S. Shen, A. F. A. Serrarens, M. Steinbuch, and F. E. Veldpaus, "Control of a hybrid driveline for fuel economy and driveability," in *Proc. ASME AVEC 2000*, Ann Arbor, MI, no. 68, pp. 469–475.